USGS
science for a changing world

U.S. DEPARTMENT OF THE INTERIOR
U.S. GEOLOGICAL SURVEY

PRELIMINARY SCIENTIFIC RESULTS OF THE CREEDE CALDERA CONTINENTAL SCIENTIFIC DRILLING PROGRAM

P.M. Bethke, Editor

Open-File Report 94-260-F

2001

SILICATE DIAGENESIS OF TUFFS IN THE CREEDE FORMATION

By

D.B. Finkelstein[1]
S.P. Altaner
R.L. Hay[2]
S. Greenberg
University of Illinois, Urbana, IL

Present addresses:
[1] Dept. of Geological Sciences, Indiana University, Bloomington, IN 47405
[2] 3420 North Alvernon Way, Tucson, AZ 85718

INTRODUCTION

The Creede Formation (Late Oligocene) contains volcaniclastic lacustrine strata that were deposited in a 2 to 3 km wide structural moat within the Creede caldera of the San Juan volcanic field. Previous studies have proposed that saline and isotopically heavy fluids from the Creede Formation were involved in ore deposition of the neighboring Creede Ag/Pb/Zn district. Tuffs from a 710 m drill core (CCM-2) and a 420 m drill core (CCM-1) were mineralogically and geochemically characterized to better understand diagenetic conditions in the Creede Formation.

METHODS

We sampled 23 tuffs (82 samples) from corehole CCM-1 (Hosselkus) and 26 tuffs (89 samples) from corehole CCM-2 (Airport) as well as volcaniclastic sandstones, breccias, and lacustrine sediments for lithologic comparisons (table 1). All samples were characterized by X-ray diffraction to determine the whole rock and clay mineralogies. Mineral abundances were calculated using mineral intensity factors from Bayliss (1986) and Reynolds (1989). Mineral morphology and paragenesis, were determined using an optical microscope, cathodoluminoscope, and JEOL JSM 840A scanning electron microscope equipped with a KEVEX 7500 energy dispersive analyzer. Mineral chemistry was determined using a CAMECA SX-50 microprobe equipped with four wavelength-dispersive X-ray chemical analyzers. A beam diameter of 5μm was used. Whole rock chemistry of tuffs was characterized by X-ray fluorescence. We calculated gains and losses of oxides in tuffs by comparing the composition of altered tuffs with unaltered tuffs and by assuming Al_2O_3 to be immobile. To account for possible volume changes associated with alteration, we calculated the density of tuff samples using XRD mineralogies and assumed mineral densities.

RESULTS

Tuffs from 0-300 m in the CCM-2 core contain the authigenic assemblage of Na/K-clinoptilolite, Al-smectite, K-feldspar, opal-CT, and less commonly illite (Figures 1, 2). The d(101) of opal-CT decreases from 4.10 Å (at 67 m) to 4.05 Å (at 193 m) (Figure 3). Below 300 m, opal-CT is recrystallized to quartz and Na/K clinoptilolite $(Na_{2.4}3K_{1.25}Ca_{0.78}Mg_{0.16})(Fe_{0.02}Al_{6.32}Si_{29.84})O_{72}\bullet 24H_2O$ converts to Na/Ca-clinoptilolite $(Na_{2.7}2K_{0.07}Ca_{1.42}Mg_{0.10})(Fe_{0.03}Al_{6.64}Si_{29.5})O_{72}\bullet 24H_2O$. Smectite, quartz, and authigenic K-feldspar increase in abundance with depth, whereas minor phases (illite ± kaolinite) decrease in

abundance (Figure 2). Na 2O increases with depth (2.5 % to 4.0 %) probably due to the greater abundance of smectite (Figures 1, 4).

Tuffs from the CCM-1 core generally contain a higher grade mineral assemblage compared to tuffs at the same depth interval in the CCM-2 core. Above 160 m in CCM-1, the tuffs contain an authigenic assemblage of Al-smectite, quartz, K-feldspar, Na/Ca-clinoptilolite ($Na_{1.88}K_{0.15}Ca_{1.64}Mg_{0.21}$)($Fe_{0.10}Al_{6.23}Si_{29.82}$)$O_{72}$•$24H_2O$, and analcime $Na_{0.84}(Fe_{0.01}Al_{0.87}Si_{2.12})O_6$•$H_2O$ with sporadic Na/Ca-heulandite as defined by a Si/Al+Fe ratio less than 4, ($Na_{2.41}K_{0.20}Ca_{1.31}Mg_{0.44}$)($Fe_{0.65}Al_{6.77}Si_{28.89}$)$O_{72}$•$24H_2O$ (Figure 5). Smectite with a minor amount (≤ 20 %) of randomly interlayered (R0) illite is the dominant clay mineral in the core. Minor amounts of regularly interstratified (R1) mixed-layer illite/smectite (I/S) with 40 to 25 % smectite layers, chlorite/smectite (C/S) with ~40 % smectite layers, and chlorite occur in the tuffs (Figure 6, 7). Percent smectite layers in I/S and C/S show no systematic variation with depth (Figure 7). Below 160 m, tuffs contain mainly Al-smectite, quartz, K-feldspar, analcime and minor randomly and regularly interstratified I/S, C/S, and chlorite. The I/S, C/S, and chlorite are more common than in the upper 160 m. Similar to CCM-2 core, tuffs from CCM-1 increases in Na 2O with depth (Figure 8). In both drillcores, volcaniclastic sandstones, mudstones and breccias have authigenic mineral assemblages similar to those in the tuffs. The minor minerals (I/S, C/S, and chlorite) are most abundant in the relatively permeable, fractured, and veined lithologies (e.g., volcaniclastic sandstones and breccias) (Figures 9, 10).

DISCUSSION

The zoning of authigenic mineral assemblages observed in CCM-2 core is characteristic of diagenetic alteration of silicic vitric tuff within an elevated geothermal gradient (Iijima and Utada, 1971; Iijima, 1988). The transition from Na/K-clinoptilolite to Na/Ca-clinoptilolite and opal-CT to quartz represents possible alteration temperatures of 45° - 57°C and 84° - 91°C, respectively (Iijima and Utada, 1971; Iijima, 1988). Assuming a surface temperature of ~0° - 4°C, erosion of 400 to 450 m of overlying rock, and an opal-CT to quartz transition temperature of 80°C, we calculate a paleogeothermal gradient of ~100°C/km. The Na/Ca-clinoptilolite to analcime transition at CCM-1 represents temperatures of 84° to 91°C. The presence of minor Na/Ca-heulandite above 160 m depth and its absence below 160 m indicates a possible transition from zone IIIa to IIIb of Iijima (1988) involving temperatures of 91° - 120°C. Because of the higher grade assemblage observed in CCM-1 core, an even higher gradient is calculated for that section (~120°C/km). We interpret the high calculated gradients to be the result of the influence of hydrothermal fluids. Evidence for high paleogradients includes the presence of minerals common to

hydrothermal alteration (R1 - I/S, R1 - C/S, and chlorite), and discontinuous changes in layer ordering and percent smectite layers in I/S and C/S with depth. Whereas gradual changes in layer ordering and percent smectite layers are observed in burial diagenetic settings (e.g., Gulf Coast sediments; Hower et al., 1976), hydrothermal terrains typically exhibit abrupt changes in mixed-layer clay mineralogy as well as the presence of both smectite and R1 - I/S (Harvey and Browne, 1991; Inoue et al., 1992).

The coexistence of two phases, smectite and R1 - I/S in both tuffs and non-tuffs, suggests the duration of alteration was less than 10,000 years (Inoue et al., 1992). Horton (1985) found that an I/S sequence extending from the Amethyst vein system in the ore district fit a 5,000 year thermal regime using the kinetic model of Pytte and Reynolds (1989).

The trends observed in CCM-2 and CCM-1 coupled with analyses of authigenic minerals are compatible with both regional diagenetic and localized hydrothermal alteration. The calculated mass balance of tuff alteration in both CCM-2 and CCM-1 involve a gain of K_2O, SiO_2, and a loss of Na_2O, MgO, MnO, and total Fe (Figures 11, 12, 13). Differences in the alkali and silica contents of secondarily hydrated and fresh glass sample pairs can be the result of exchange with groundwater (Noble, 1967). The calculated gains and losses are attributed to diagenetic and localized hydrothermal alteration. Chemical analyses of clinoptilolite appear to indicate the degree of alteration in outcrop and in the CCM-2 and CCM-1 drillcores (table 2). The clinoptilolites in CCM-2 above 300 m depth have Si/(Al+Fe) ranging 4.72 - 4.98, whereas those below 300 m and those from CCM-1 range from 4.40 - 4.64 (table 2). The extraframework cations appear to be particularly sensitive to the fluid with which they last equilibrated (Figure 14). The outcrop samples plot away from the two major fields and have had Na and some K replaced by Ca and Mg. Clinoptilolites in CCM-2 above 300 m depth plot in the opal-CT - clinoptilolite field, whereas those below 300 m and those from CCM-1 plot in the clinoptilolite - K-feldspar field (Figure 15).

The observed silicate mineralogies do not support the Creede Formation as a source for saline and isotopically heavy fluids. For example, the presence of clinoptilolite and absence of Al-rich zeolites (erionite, phillipsite) suggest pore waters of moderate pH (7-9) and relatively low Na/K ratio (Mariner and Surdam, 1970; Barth-Wirsching and Höller, 1989). In addition, we do not observe other minerals common to evaporite basins (e.g., saline minerals and Mg-rich phyllosilicates). Using a calculation procedure described in Boles and Surdam (1979) that involves comparison of exchangeable cation composition of clinoptilolite and pore fluid compositions, we estimate that the clinoptilolite last equilibrated with water of: low TDS (1257 - 1575 ppm), Na+K/Ca+Mg = 3.6 - 5.6, and a pH of about 8 (table 3).

The diagenetic silicate mineralogies contrast with isotopic data from the lacustrine carbonates which suggest evaporative conditions. Future work on the isotopic composition of authigenic silicates and carbonates will provide information about the nature of the lake water and the evolution of pore fluids.

REFERENCES

Barth-Wirsching, Ulrike and Helmut Höller, 1989, Experimental studies on zeolite formation conditions: European Journal of Mineralogy, v. 1, pp. 1448-1462.

Bayliss, P., 1986, Quantitative analysis of sedimentary minerals by powder X-ray diffraction: Powder Diffraction, 1, pp. 37-39.

Boles, J.R., and R.C. Surdam, 1979, Diagenesis of volcanogenic sediments in a Tertiary saline lake, Wagon Bed Formation, Wyoming: Amer. J. Sci., 279, pp. 832-853.

Harvey, C.C. and P.R.L. Browne, 1991, Mixed-layer clay geothermometry in the Wairakei Geothermal Field, New Zealand, Clays and Clay Minerals, v. 39, 614-621.

Horton, D.G., 1985, Mixed-layer illite/smectite as a paleotemperature indicator in the Amethyst vein system, Creede district, Colorado, U.S.A.: Contrib. Min. Pet., v. 91, pp. 171-179.

Hower, J., Eslinger, E., Hower, M., and E. Perry, 1976, Mechanism of burial metamorphism of argillaceous sediment: 1) mineralogical and chemical evidence: Geol. Soc. Am. Bull., v. 87, pp. 725-737.

Iijima, A., 1988, Diagenetic transformations of minerals as exemplified by zeolites and silica minerals - A Japanese view: in Diagenesis II, G.V. Chilingarian and K.H. Wolf, eds., Developments in Sedimentology, v. 43, pp. 147-212.

Iijima, A., and M. Utada, 1971, Present-day zeolitic diagenesis of the Neogene geosynclinal deposits in the Niigata oil field, Japan: in Molecular Sieve Zeolites, 1 (Advances in Chemistry Series, 101) Am. Chem. Soc., pp. 548-555.

Inoue, A., M. Utada, and K. Wakita, 1992, Smectite - to - illite conversion in natural hydrothermal systems: Applied Clay Science, v. 7, pp. 131-145.

Mariner, R.H., and R.C. Surdam, 1970, Alkalinity and formation of zeolites in saline/alkaline lakes: Science,v. 170, pp. 977-980.

Noble, D.C., 1967, Sodium, potassium, and ferrous iron contents of some secondarily hydrated natural silicic glasses: American Mineralogist, v. 52, pp. 280-286.

Pytte, A.M., and R.C. Reynolds, 1989, The thermal transformation of smectite to illite: in Thermal History of Sedimentary Basins, N.D. Naeser and T.H. McCulloh, eds., pp. 133-140.

Ratté, J.C., and T.A. Steven, 1967, Ash flows and related volcanic rocks associated with the Creede caldera, San Juan mountains, Colorado: Geological Survey Professional Paper, 524-H, 58 p.

Reynolds, R.C., 1989, Principles and techniques of quantitative analysis of clay minerals by X-ray powder diffraction: in Quantitative Mineral Analyses of Clays, D.R. Pevear and F.A. Mumpton, eds., pp. 4-36.

FIGURE CAPTIONS

Figure 1. Normalized weight percent abundance of authigenic silicates from tuffs in the CCM-2 drillcore. Primary quartz and K-feldspar are present in the upper part of the core (0 - 300 m). Below 300 m, secondary quartz and K-feldspar are more abundant.

Figure 2. Normalized weight percent abundance of clay minerals in the < 0.5 μm size fraction from tuffs in the CCM-2 drillcore.

Figure 3. Opal-CT [101] d-spacing decreases from ~4.1 Å to 4.05 Å with depth in the CCM-2 drillcore. Below 300 m, opal-CT is recrystallized to quartz.

Figure 4. Weight percent Na2O increases with depth possibly due to the greater abundance of smectite and analcime.

Figure 5. Normalized weight percent abundance of authigenic silicates from tuffs in the CCM-1 drillcore.

Figure 6. Normalized weight percent abundance of clay minerals in the < 0.5 μm size fraction from tuffs in the Hosselkus drillcore.

Figure 7. Percent expandable (smectite) in clays in the < 0.5 μm size fraction from tuffs in the Hosselkus drillcore. The dominant phase is smectite with minor I/S and C/S.

Figure 8. Weight percent Na2O increases with depth possibly due to the greater abundance of smectite, analcime, and primary plagioclase.

Figure 9. Normalized weight percent abundance of clay minerals in the < 0.5 μm size fraction from volcaniclastic sandstones, mudstones, and breccias in the Hosselkus drillcore.

Figure 10. Percent expandable (smectite) in clays in the < 0.5 μm size fraction from volcaniclastic sandstones, mudstones, and breccias in the Hosselkus drillcore. The dominant phase is smectite with minor I/S and C/S.

Figure 11. Calculated % gain/loss of Na2O vs K2O in tuffs with Al2O3 assumed immobile.

Figure 12. Calculated % gain/loss of total Fe (Fe2O3) vs SiO2 in tuffs with Al2O3 assumed immobile.

Figure 13. Calculated % gain/loss of MnO vs MgO in tuffs with Al2O3 assumed immobile.

Figure 14. Ternary diagram of extraframework cations of clinoptilolite in shards from outcrop, CCM-2, and CCM-1.

Table 1. Silicate Diagenesis of Tuffs in the Creede Formation. Sampled Lithologies from Drillcore

- Tuffs 23 tuffs from CCM-1 (82 samples) 26 tuffs from CCM-2 (89 samples)
- Lacustrine pelletal carbonate (40 samples)
- Tuffaceous siltstone and sandstone (51 samples)
- Conglomerate (11 samples)
- Breccias (43 samples)
- Ashflows (20 samples)

X-Ray Diffraction Analysis

- 312 Whole Rock samples - micronized (including 180 heat treatments)
- 286 Clay size-fractions (untreated, glycolated, heated)

Scanning Electron Microscope

- Hosselkus: Tuffs (42 samples)
  Lacustrine carbonates (15 samples)
  Sandstones and Siltstones (10 samples)
  Breccias (6 samples)

- Airport: Tuffs (51 samples)
  Lacustrine carbonates (6 samples)
  Sandstones and Siltstones (6 samples)
  Breccias (3 samples)
  Ashflow (4 samples)

Petrography and Cathodoluminescence

- Hosselkus: 74 thin sections

- Airport: 132 thin sections

X-Ray Fluorescence - Tuffs (bulk samples)

- Hosselkus: 6 thick tuffs (>15 cm thickness), 22 samples
  5 thin tuffs (<15 cm thickness)

- Airport: 6 thick tuffs (>15 cm thickness), 23 samples
  4 thin tuffs (<15 cm thickness)

Microprobe

- Hosselkus: 1 sandstone - shards (9 analyses; edge, middle, center)
  2 tuffs - shards (22 analyses; edge, middle, center)

- Airport: 5 tuffs - pores, shards, fracture fills, feldspars
  (74 analyses; edge, middle, center)

Table 2. SELECTED CLINOPTILOLITE FORMULAE:

	Si/(Al+Fe) *	(Na+K)/(Ca+Mg) *
Outcrop - Dry Gulch		
$(K_{.67}Ca_{2.40}Mg_{.28})(Si_{29.48}Al_{6.69})O_{72} \bullet 24H_2O$	4.24 - 4.81	0.24 - 0.93
CCM-2 - 67.7 m		
$(Na_{2.46}K_{1.20}Ca_{.83}Mg_{.17})(Si_{29.92}Al_{6.18}Fe_{.03})O_{72} \bullet 24H_2O$	4.72 - 4.98	2.29 - 4.19
CCM-1 - 129.4 m		
$(Na_{3.22}K_{.19}Ca_{1.27}Mg_{.15})(Si_{29.42}Al_{6.55}Fe_{.14})O_{72} \bullet 24H_2O$	4.40 - 4.64	1.58 - 2.41

* range of all analyses.

Table 3. BRINE COMPOSITION BASED ON EXTRAFRAMEWORK CATIONS OF CLINOPTILOLITE

METHOD AFTER BOLES AND SURDAM, 1979

	Na + K	Ca	Mg	TDS	pH
Airport	**85**	**11**	**4**	**1575**	**8**
Hosselkus	**79**	**14**	**8**	**1257**	**8**

Avg. mole % normalized to 100%

Figure 1. Airport Tuffs Normalized Weight Percent Abundance Authigenic Silicates

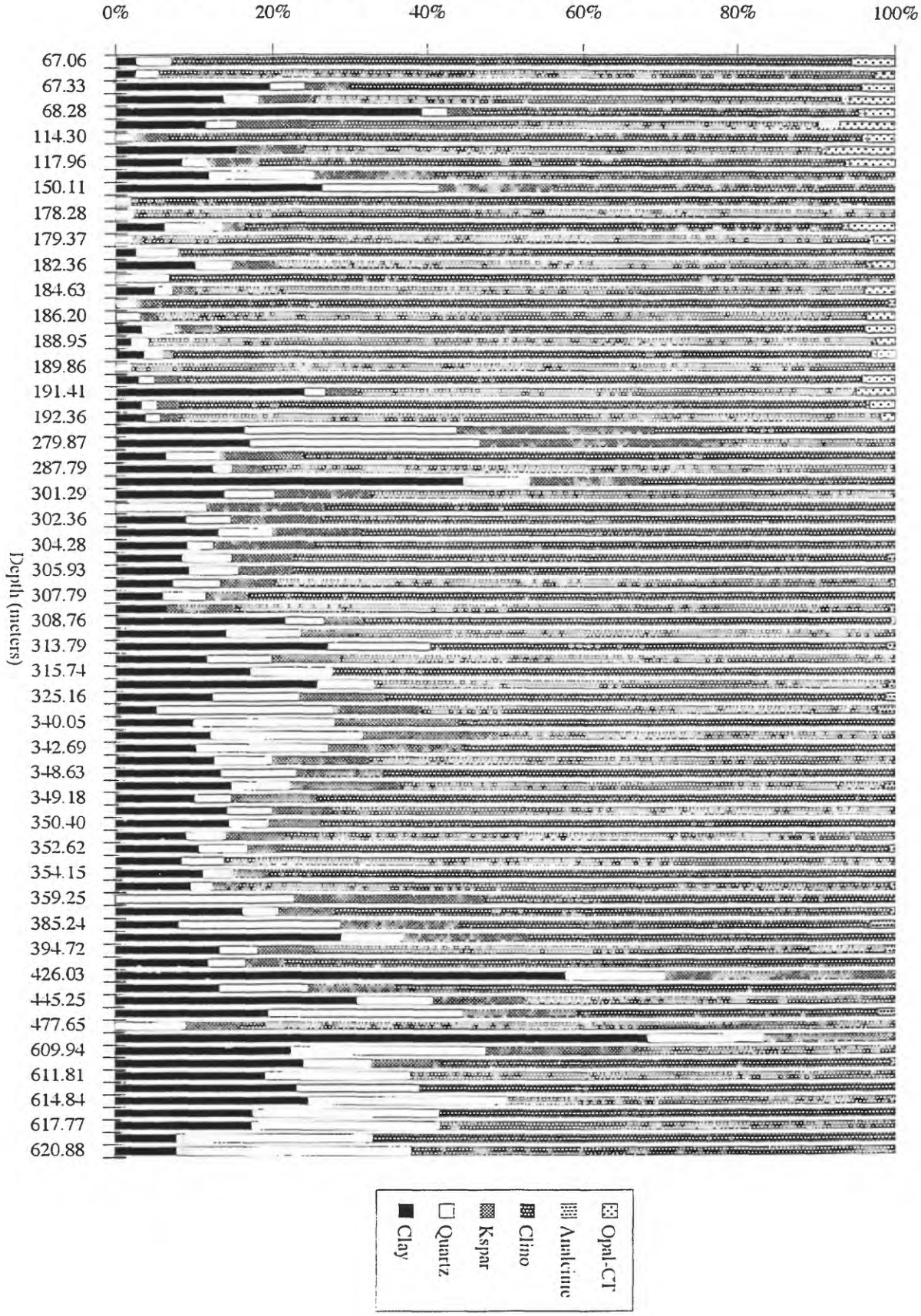

Figure 2. Airport Tuffs Normalized Weight Percent Abundance Clay Minerals (<0.5μ, glycolated)

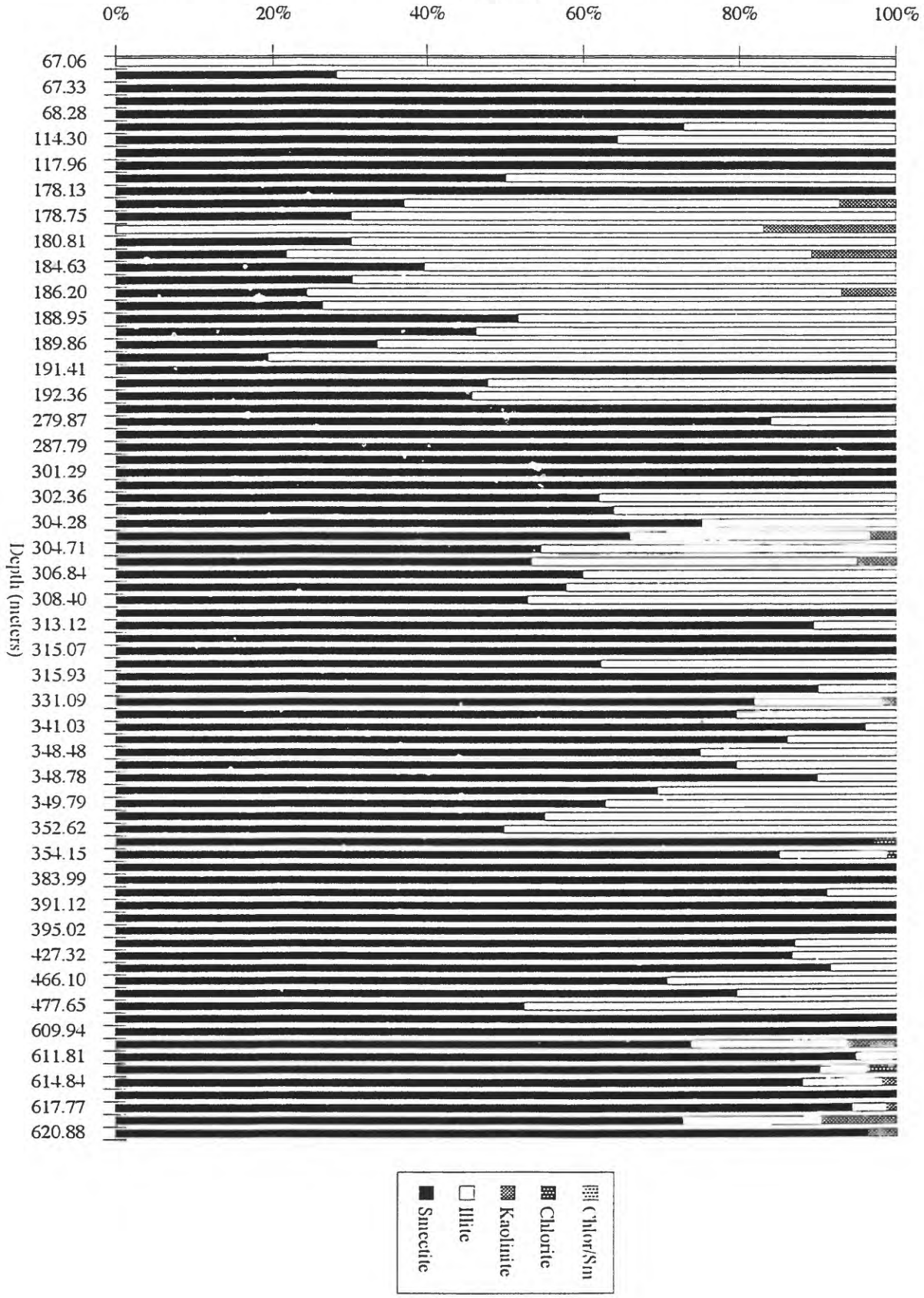

Figure 3. Airport Tuffs Opal-CT [101] d-spacing (Å)

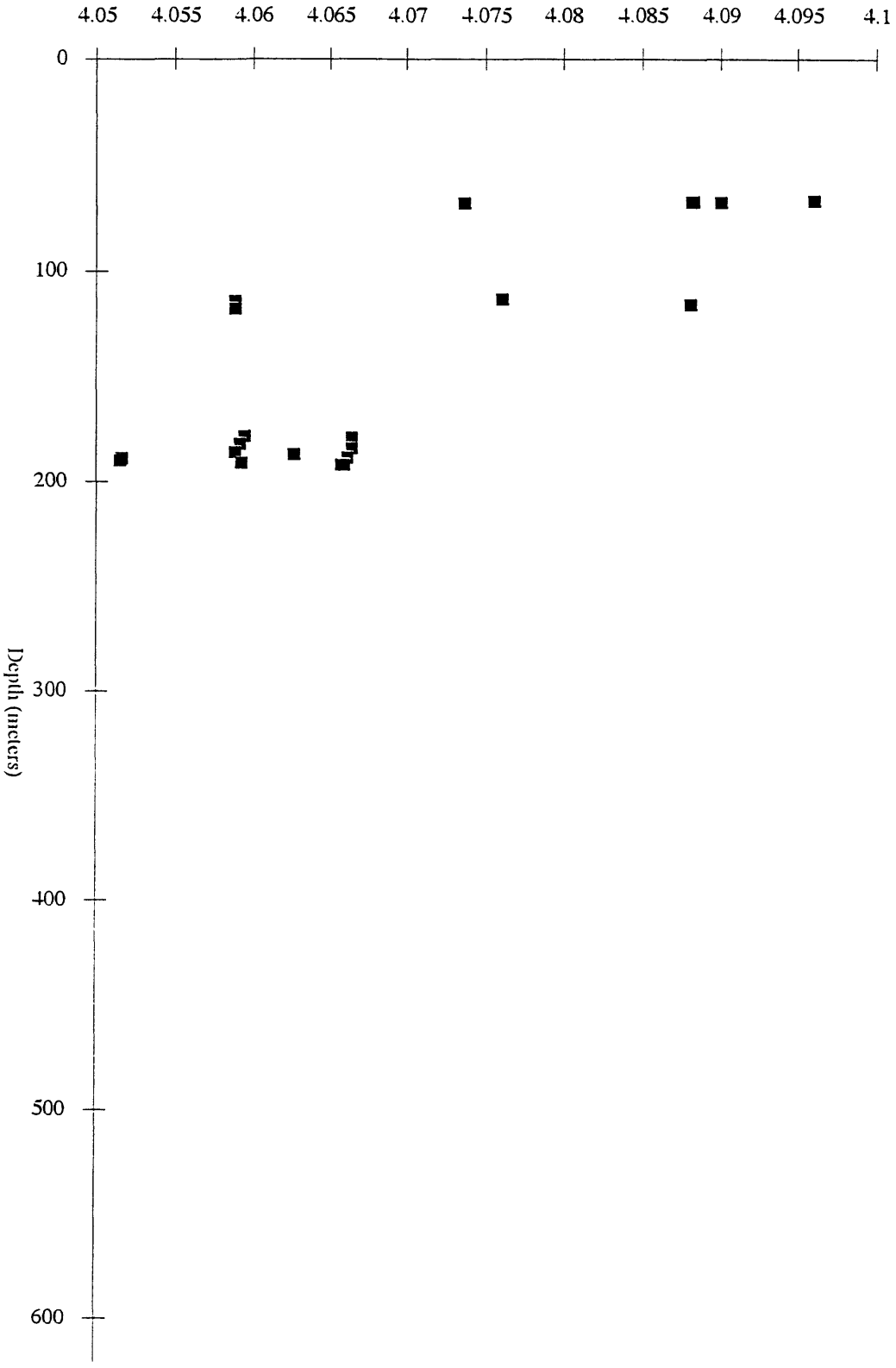

Figure 4. Weight Percent Na2O Airport Tuffs (Bulk)

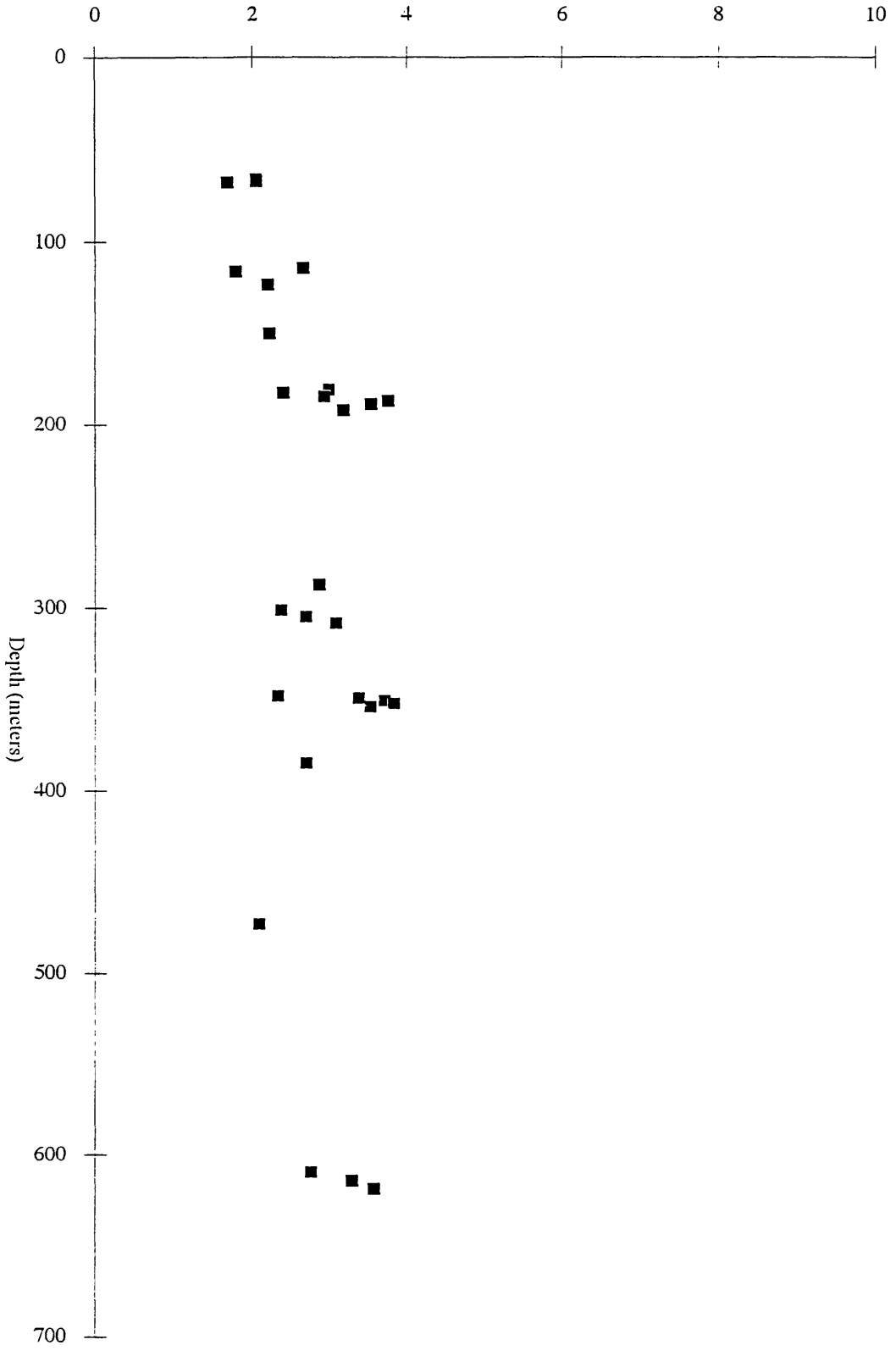

Figure 5. Hosselkus Tuffs Normalized Weight Percent Abundance Authigenic Silicates

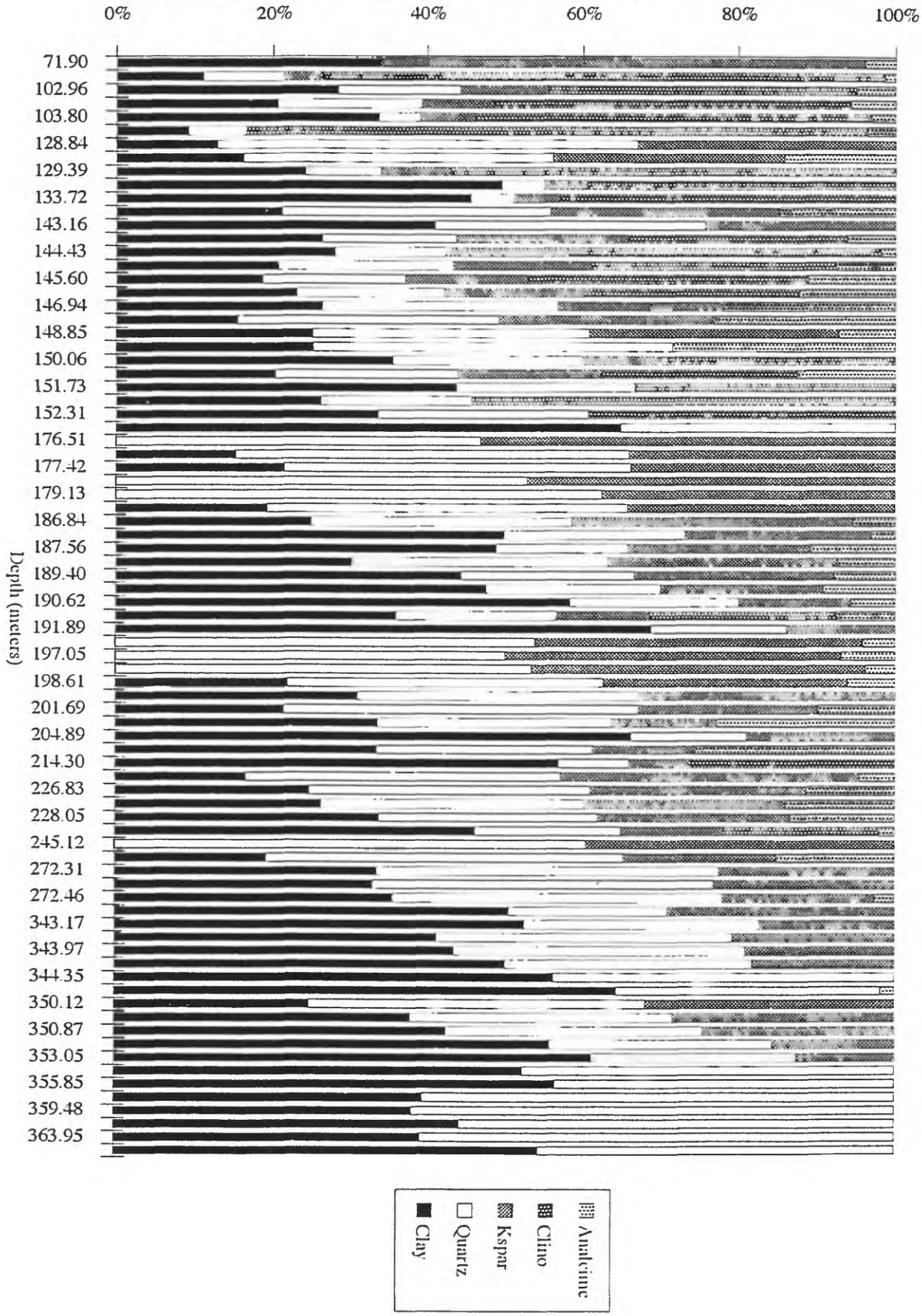

Figure 6. Hosselkus Tuffs Normalized Weight Percent Abundance Clay Minerals (<0.5μ, glycolated)

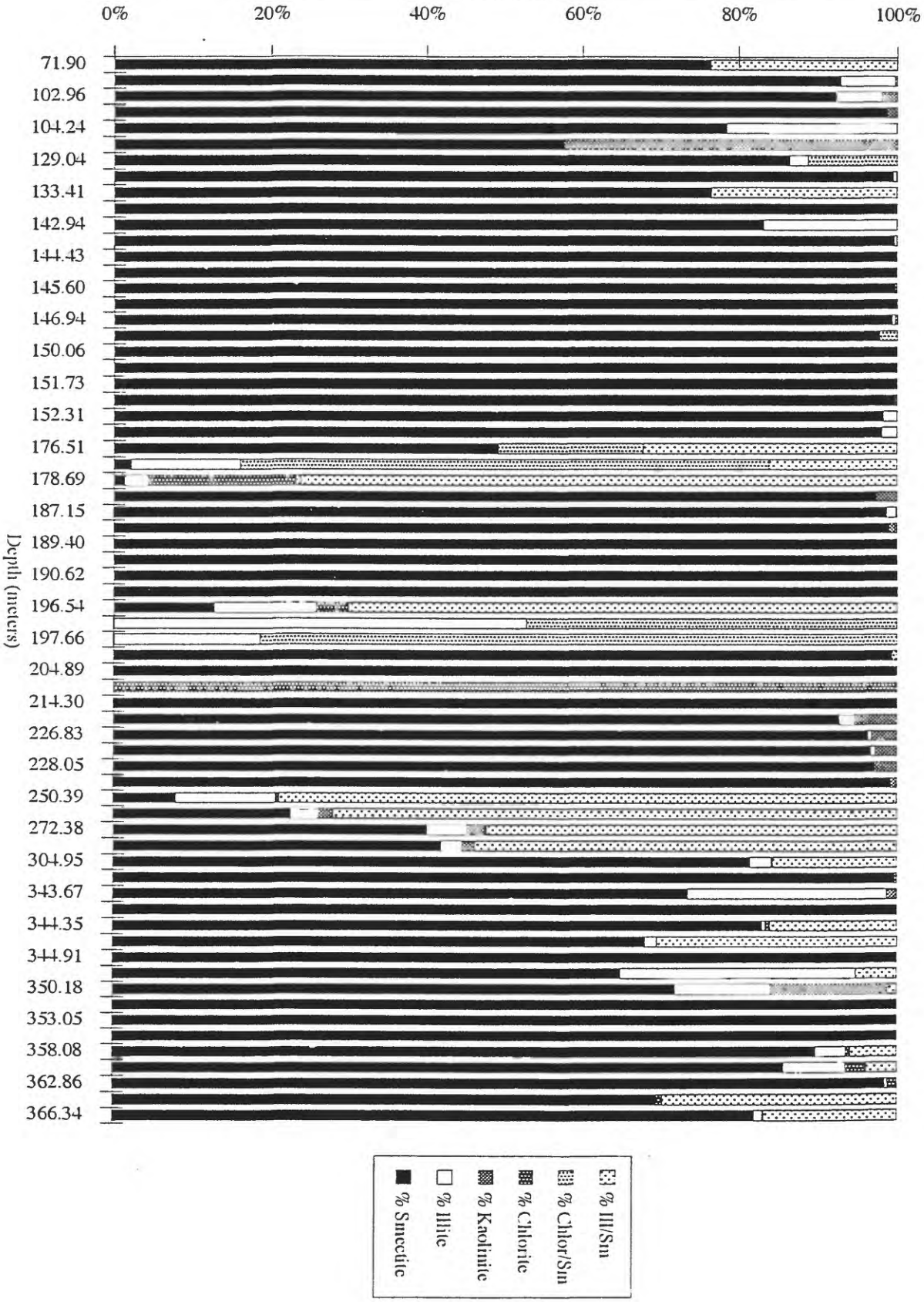

Figure 7. Hosselkus Tuffs Percent Expandable (<0.5μ, glycolated)

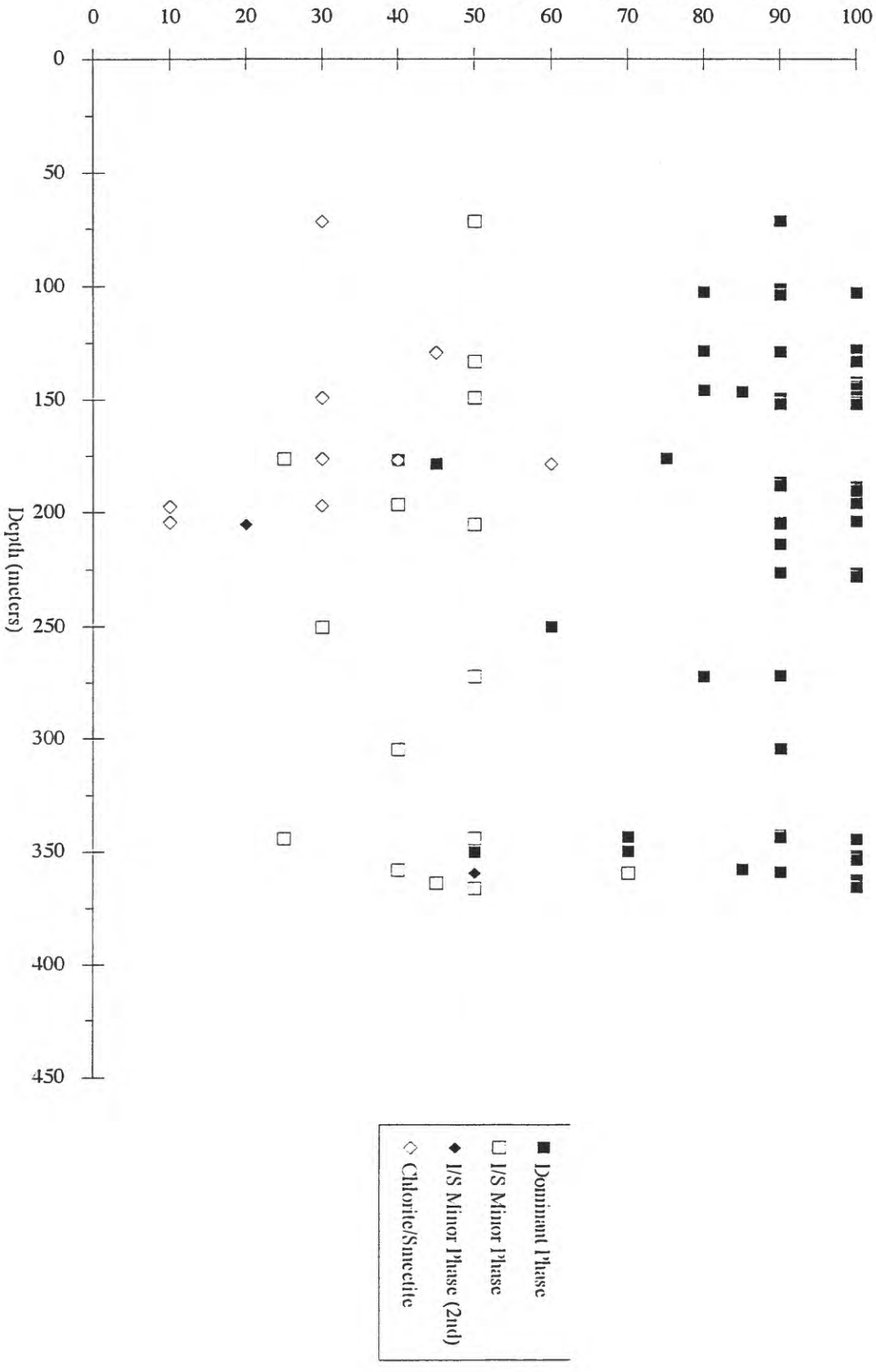

Figure 8. Weight Percent Na2O Hosselkus Tuffs (Bulk)

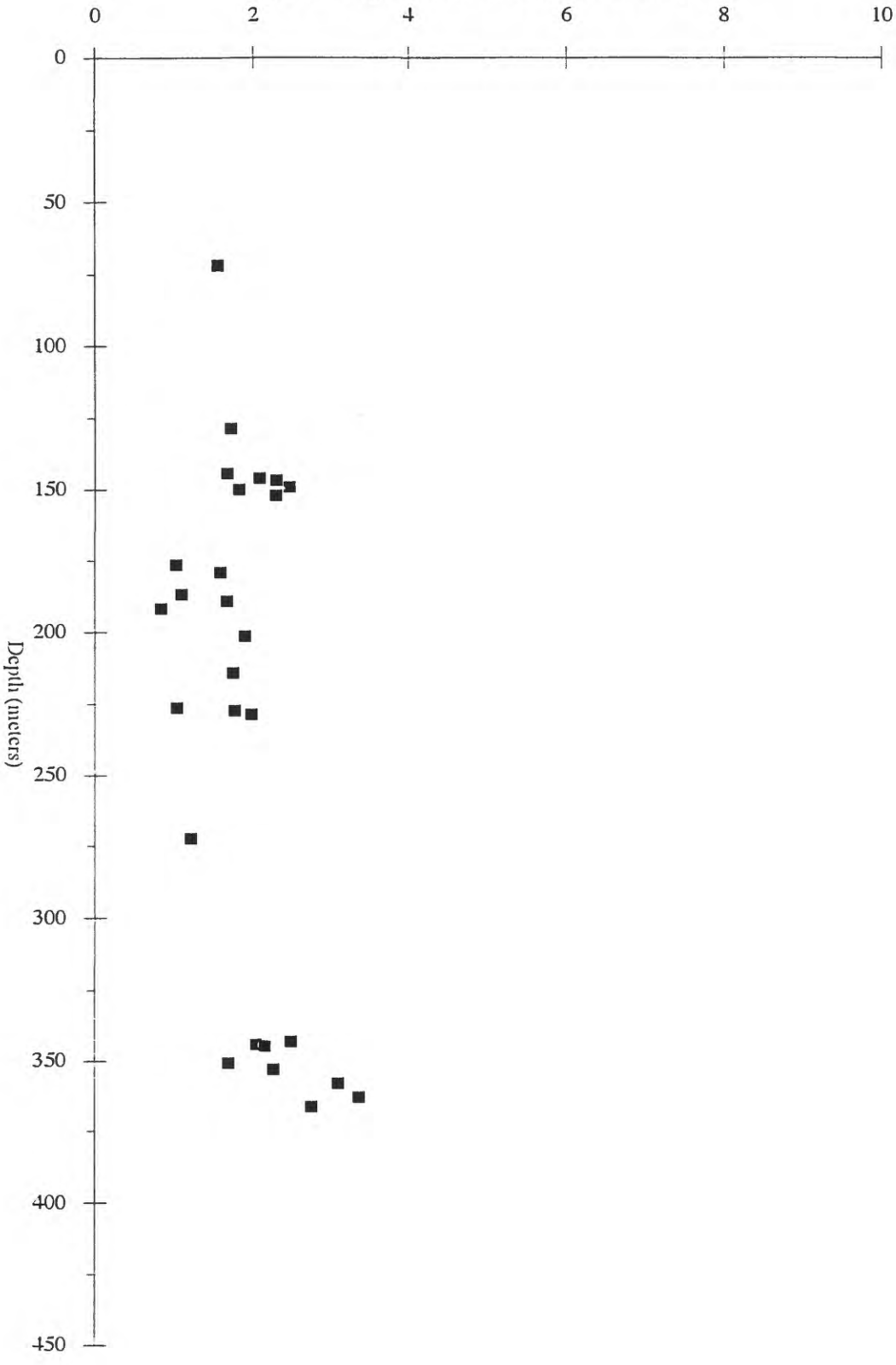

Figure 9. Hosselkus Non-Tuffs Normalized Weight Percent Abundance Clay Minerals
(<0.5μ, Glycolated)

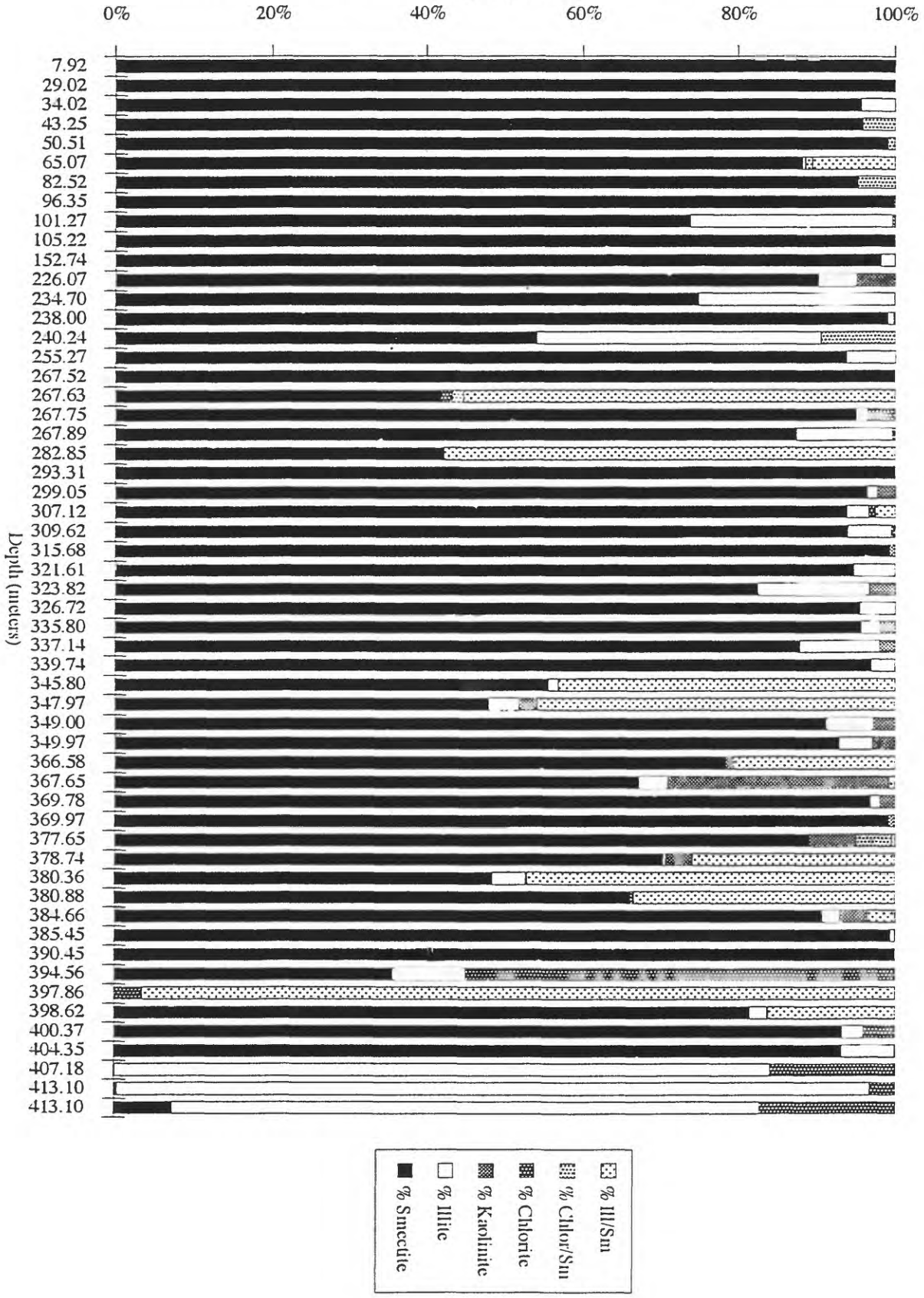

Figure 10. Hosselkus Non-Tuffs Percent Expandable (<0.5μ, glycolated)

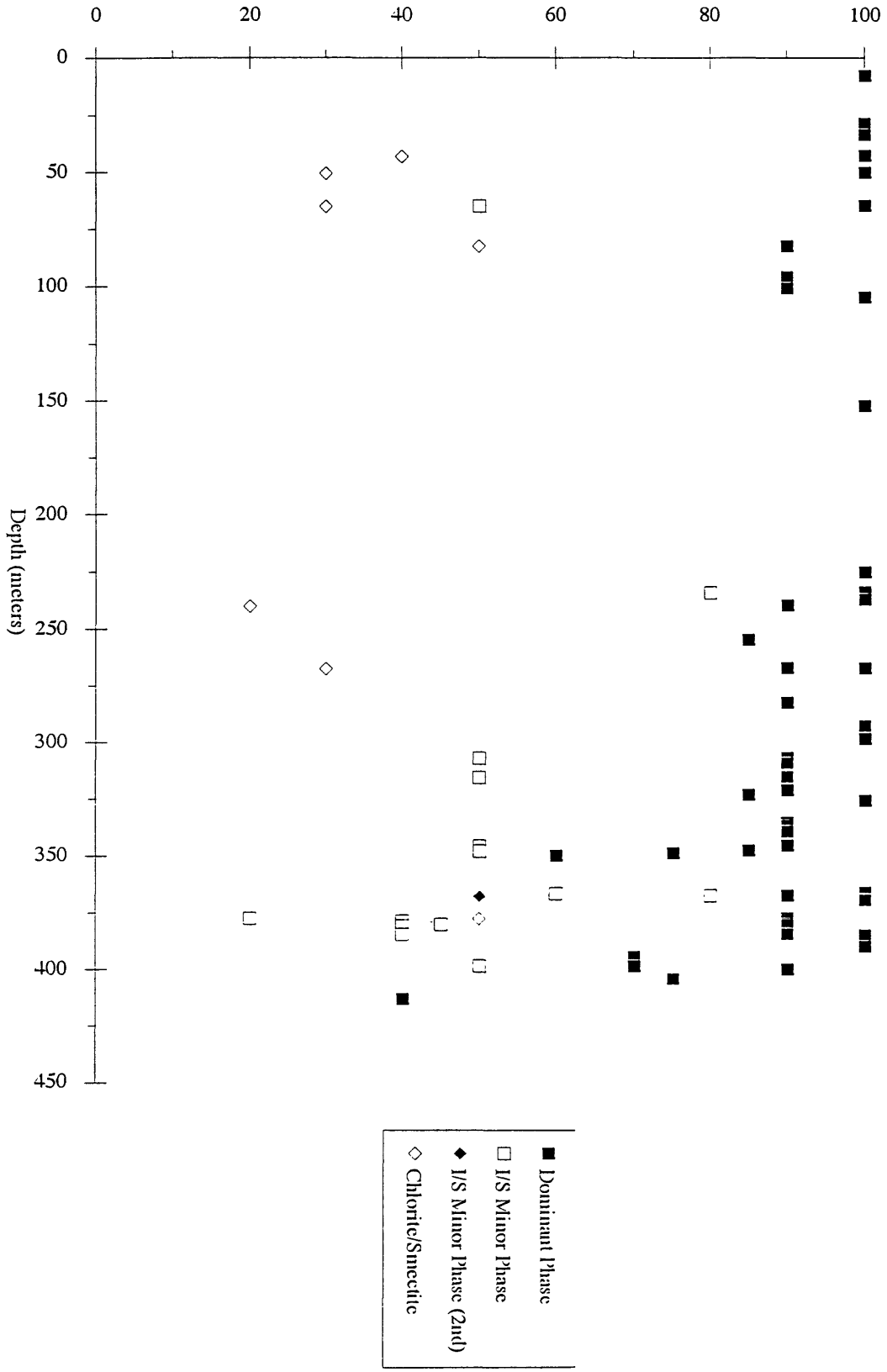

Figure 11. % Gain/Loss of Tuffs vs. Fisher Quartz Latite (Na2O vs K2O)

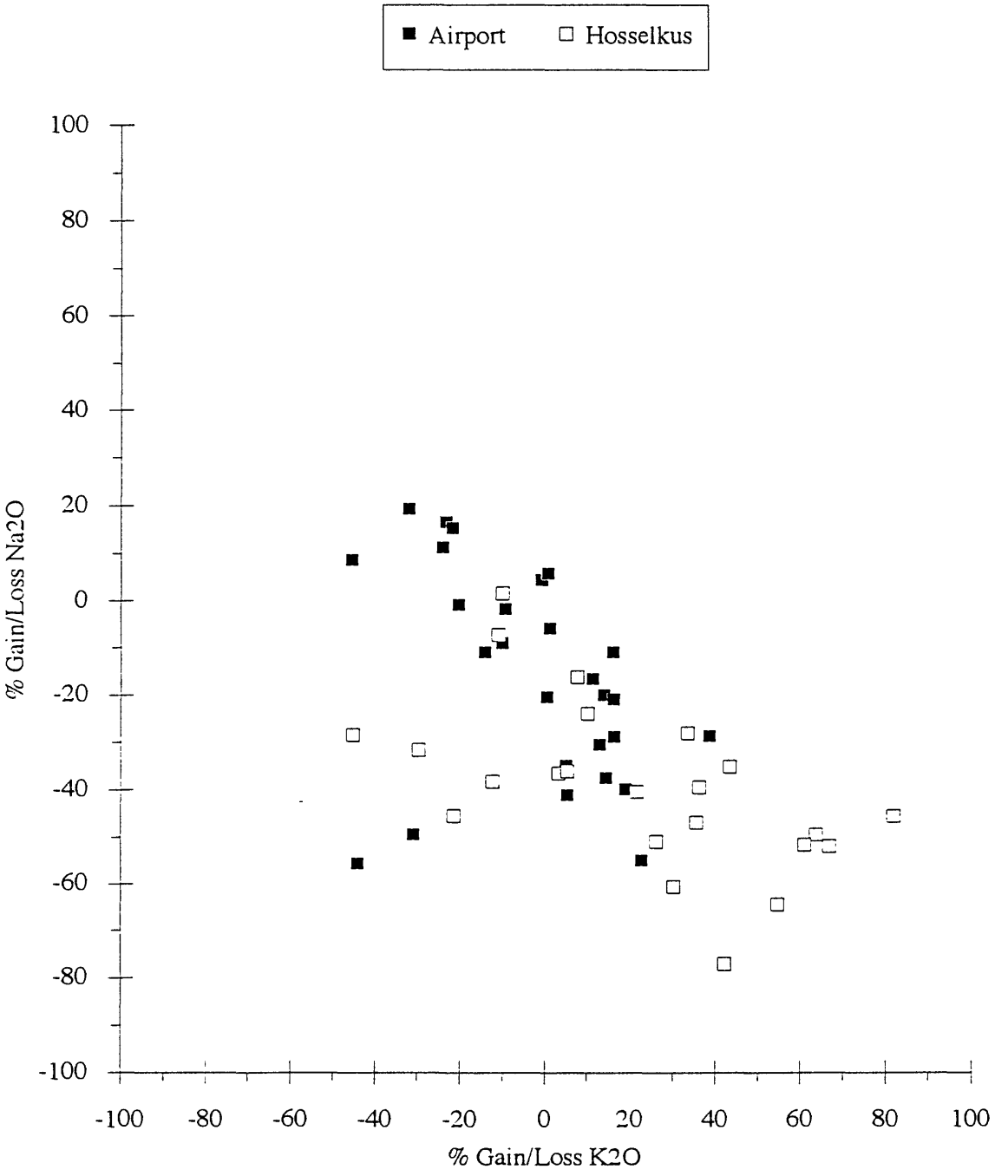

Figure 12. % Gain/Loss of Tuffs vs. Fisher Quartz Latite (Fe2O3 vs SiO2)

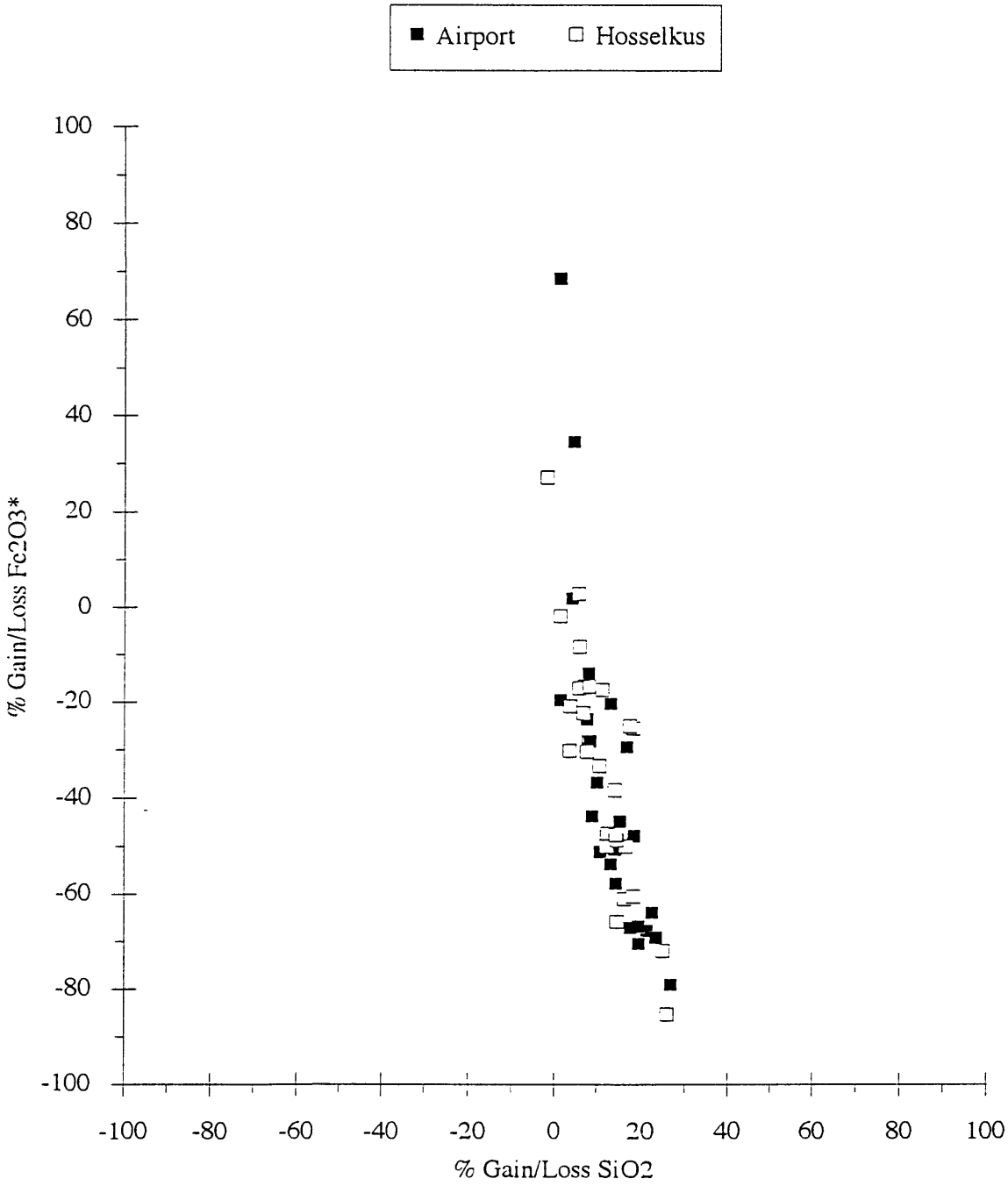

Figure 13. % Gain/Loss of Tuffs vs. Fisher Quartz Latite (MnO vs MgO)

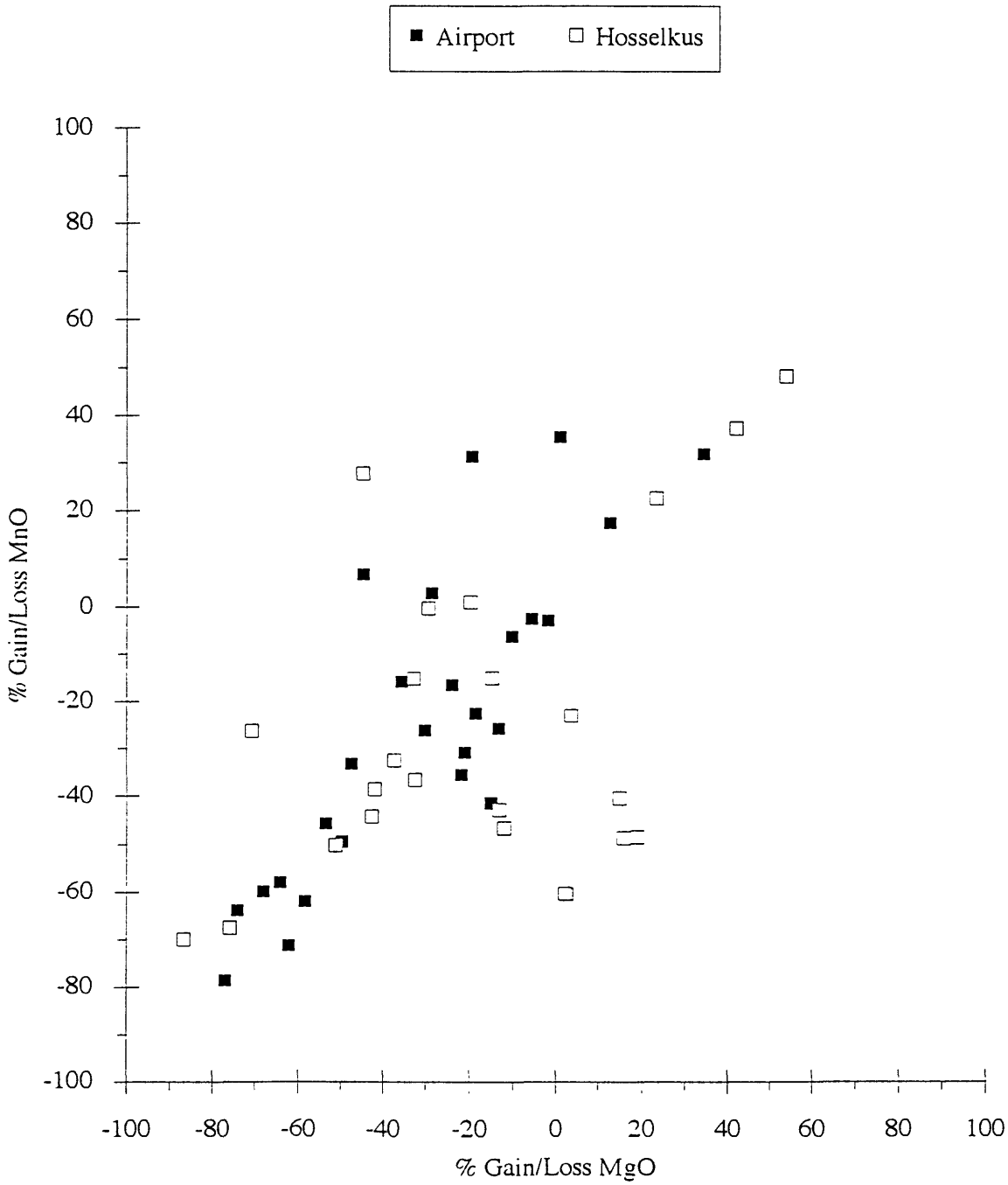

Figure 14. Clinoptilolite: Extraframework Cations (representative analyses)

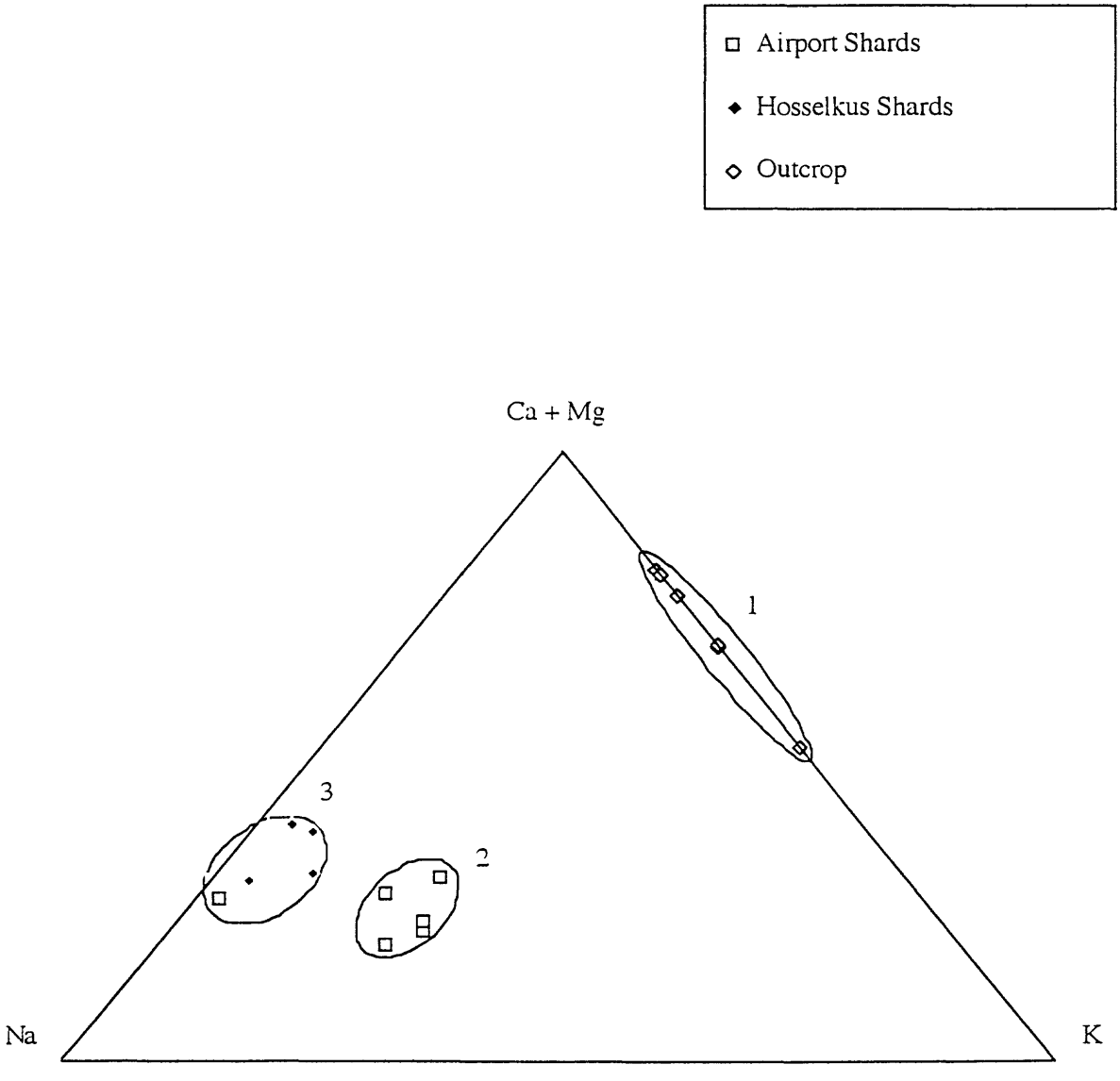

1 Outcrop.
2 Airport, opal-CT - clinoptilolite zone.
3 Hosselkus and Airport, clinoptilolite - authigenic kspar zone.